Power Loss Estimation in *LLC* Synchronous Rectification Using Rectifier Current Equations

Ettore Scabeni Glitz, *Student Member, IEEE*, Jhih-Da Hsu, *Student Member, IEEE*, and Martin Ordonez, *Member, IEEE*

***Abstract*—In past years, *LLC* resonant converters have become a mainstream topology for dc–dc power conversion due to their advantages, such as the superior efficiency obtained with the soft switching of MOSFETs. In order to further improve the efficiency of the converter, synchronous rectification (SR) can be implemented as an alternative for diode rectification. As a result, the vast majority of the literature related to this field of study presents different *LLC* SR control algorithms, which aim to improve the operation of the rectification. Unlike prior work on SR controllers, this paper contributes to the area of power loss estimation using rectifier current equations (RCE). The developed method based on time-domain analysis of SR currents provides a new analytical framework to characterize the behavior of SR. Implications in SR power losses of different time delays are investigated using the developed loss estimation method. In addition, different converter design parameters, such as choice of inductance ratio, can be analyzed. The RCE captures the true discontinuous and complex behavior of SR, which is often oversimplified by the conventional first-harmonic approximation (FHA). As a result, the proposed method facilitates the design of *LLC* resonant converters and provides increased precision in SR power loss estimation when compared to FHA, and in a considerably faster fashion when compared with precise yet computationally intensive simulation software. This paper is validated with simulation and experimental results.**

***Index Terms*—First harmonic approximation, *LLC* resonant converter, *LLC* synchronous rectification (SR), MOSFET design tool, power losses, SR.**

I. Introduction

RESONANT converters present advantages that favor the efficiency of these topologies due to the soft-switching of active components [1], [2]. *LLC* converters, in particular, present characteristics such as wide output voltage regulation and low electromagnetic interference, which are of interest for applications such as electric vehicle battery charging [3]–[5], renewable energy generation [6], and low-power applications [7], [8]. In order to further improve the efficiency of this topology, numerous techniques for implementing synchronous rectification (SR) are presented in the literature, ranging from simple control algorithms with minimized sensing requirements [9]–[13] to more complex control schemes, which rely on drain current (i_D) sensing [14]–[19] or drain–source voltage (v_{DS}) measurement [20].

The different control approaches available in the literature aim to minimize power losses of the switches (P_{mos}), since these negatively impact on the efficiency of the converter and produce heat, which compromises the durability of the equipment [21], [22]. In fact, designing the thermal management of active components is one of the most important aspects of prototype design and relies on the accurate determination of P_{mos} before the converter is built [23]. However, since time constants of thermal and electrical phenomena are considerably different, simulation of P_{mos} can be computationally intensive, demanding hours or even days of uninterrupted simulations. As an alternative, steady-state analysis using first-harmonic approximation (FHA) or time-domain expressions for *LLC* resonant converters [24]–[30] can be employed for substantially faster P_{mos} determination. Nevertheless, the application of this method in SR P_{mos} has yet to be fully analyzed. There are also opportunities for investigating the impact on P_{mos} of operating conditions such as current delivered to load (I_{load}) and different control techniques resulting in various turn-ON and turn-OFF delays (t_d), as well as different design considerations such as the inductance ratio (m), which is defined as the relationship between the magnetizing inductance (L_m) and series resonant inductance (L_r).

In order to implement increasingly efficient *LLC* SR techniques, plenty of literature is available on novel control algorithms. Unlike most of *LLC* SR papers, this paper presents a method for estimating losses in the SR of the topology, which has not been thoroughly analyzed yet. While FHA is the established tool for analyzing the behavior of resonant converters, it oversimplifies key waveforms necessary for power loss estimation. The presented method, based on rectifier current equations (RCE), introduces a fast and precise algorithm that allows for the determination of *LLC* SR power losses before the converter is built. This method accounts for different operating conditions and design considerations of the converter. As a result, it enables the investigation of the behavior of P_{mos} for several existing SR algorithms as different design characteristics are implemented. The electrical behavior of the SR current and P_{mos}

Manuscript received December 5, 2018; revised April 15, 2019; accepted May 3, 2019. Date of publication May 22, 2019; date of current version January 3, 2020. This work was supported by the Natural Sciences and Engineering Research Council of Canada (NSERC). *(Corresponding author: Ettore Scabeni Glitz.)*

The authors are with the Department of Electrical and Computer Engineering, The University of British Columbia, Vancouver, BC V6T 1Z4, Canada (e-mail: ettoreglitz@ieee.org; danielhsu@ece.ubc.ca; mordonez@ieee.org).

Color versions of one or more of the figures in this paper are available online at http://ieeexplore.ieee.org.

Digital Object Identifier 10.1109/TIE.2019.2917372

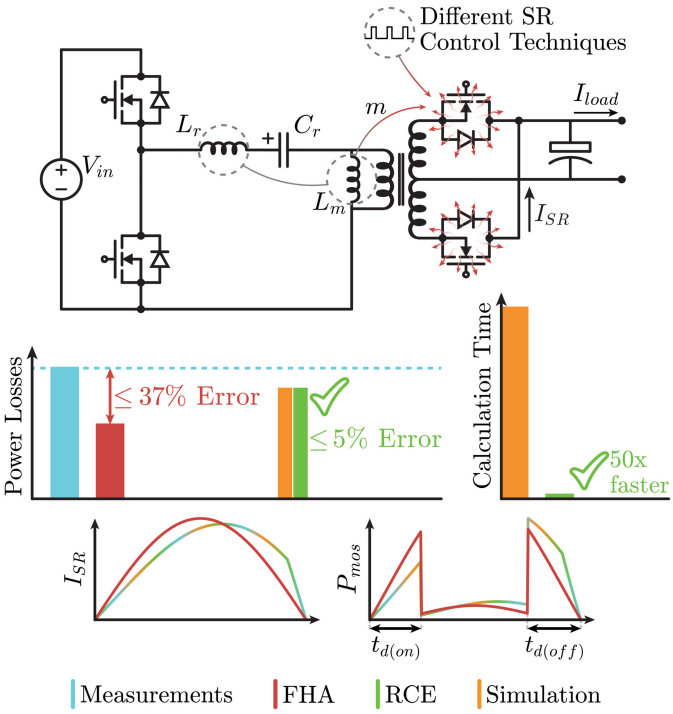

Fig. 1. Proposed RCE method is a tool for estimating SR losses with increased precision when compared to FHA. The developed method accounts for different operating conditions and design parameters, in a process that is 50 times faster than simulation software.

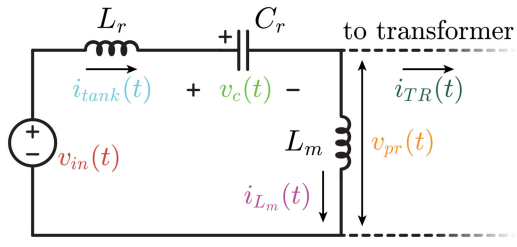

Fig. 2. Equivalent circuit for the primary of the *LLC* resonant converter.

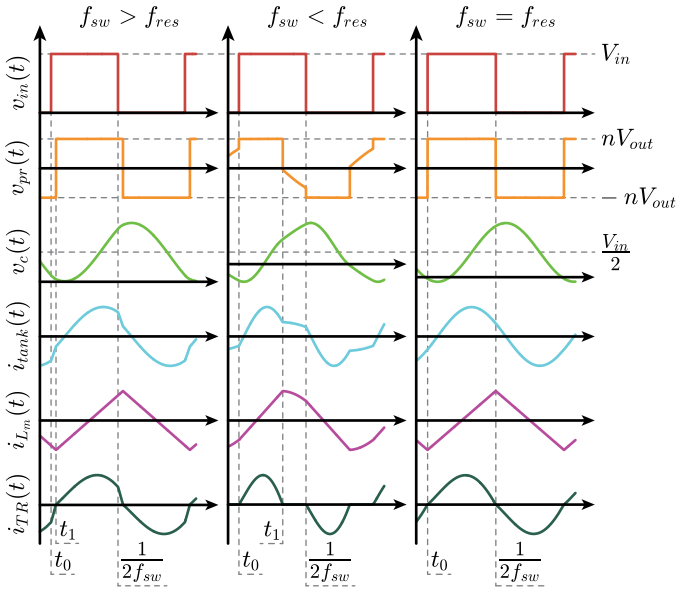

Fig. 3. Waveforms for operation of the *LLC* converter when $f_{\rm sw} > f_{\rm res}$ (left), $f_{\rm sw} < f_{\rm res}$ (middle), and $f_{\rm sw} = f_{\rm res}$ (right). Since the observed $i_{\rm TR}(t)$ is not sinusoidal, approximation by FHA will poorly reflect the behavior of the topology.

determination as predicted by RCE is verified by simulation and experimental results. Improved correlation with expected results is obtained when compared to the well-established but oversimplified FHA, as Fig. 1 shows. In addition, $P_{\rm mos}$ determination is realized around 50 times faster using RCE when compared with simulation software. This allows for the analysis of various operating conditions, in a process that would be unfeasible using simulation software. Section II develops and experimentally verifies the required time-domain equations necessary for the computing of $P_{\rm mos}$. In Section III, turn-ON and turn-OFF delays are incorporated into the calculation of $P_{\rm mos}$, revealing the most critical delay conditions that result in increased losses. Section IV analyzes the impact on $P_{\rm mos}$ of different inductance ratio design and compares the obtained values with that calculated using FHA. Finally, experimental measurements validate the proposed method, presenting a reduction from 12 to 2% in an average error for loss estimation when compared to FHA.

II. Rectifier Current Equations for *LLC* SR

Simulation of thermal phenomena in high-frequency converters requires substantial computational resources, since a small time-step must be employed for long periods of simulation time. As an alternative, steady-state time-domain equations, which predict the behavior of the converter under different operating conditions and design parameters, can be used to assess thermal behavior in a timely fashion and without the need of specific simulation software. The electrical behavior of the converter is extracted from the time-domain equations, which can also be used for the determination of $P_{\rm mos}$. The thermal behavior can then be extracted using the simplified thermal model of a MOSFET.

While FHA is the established tool for determining the behavior of resonant converters, it oversimplifies the obtained waveforms to such a degree that they are not useful for power loss analysis. As an alternative, RCE allows for the determination of $i_{\rm SR}(t)$ based on its operating conditions and design characteristics, reflecting the actual behavior of the topology. Considering the converter shown in Fig. 1, the circuit connected to the primary of the transformer can be represented by that shown in Fig. 2.

In order to determine losses in the SR of *LLC* resonant converters, the current that flows through the SR MOSFETs ($i_{\rm SR}(t)$) must be determined. This current is derived from the rectified current, which comes from the current that flows through the transformer ($i_{\rm TR}(t)$). This current can be determined by the difference between the current that flows through the tank of the converter ($i_{\rm tank}(t)$) and the current that flows through the magnetizing inductance ($i_{L_m}(t)$). As shown in Fig. 3, the behavior of the converter depends on the switching behavior of the

inverter MOSFETs with respect to the resonant frequency (f_{res}) of the tank: above, below, or at resonant frequency.

A. Operation Above the Resonant Frequency

Fig. 3 shows the general behavior of the waveforms of the circuit shown in Fig. 2 when it operates above the resonant frequency, considering a duty cycle of $D = 0.5$. It is possible to observe that the average value of $v_C(t)$ is $\frac{V_{\text{in}}}{2}$, since the primary of the *LLC* converter is a half-bridge topology. The average of the currents $i_{\text{tank}}(t)$ and $i_{L_m}(t)$ is zero. At $t = t_0 = 0$, $v_{\text{in}}(t)$ assumes the value V_{in}, which is maintained until $t = \frac{1}{2f_{\text{sw}}}$. The voltage across the primary windings of the transformer is at $-nV_{\text{out}}$ when $t = t_0$ and changes to nV_{out} at the time instant $t = t_1$. Therefore, the behavior of the converter can be analyzed based on two time intervals: from $t = t_0$ to $t = t_1$ and from $t = t_1$ to $t = \frac{1}{2f_{\text{sw}}}$. For $0 < t < t_\phi$, $i_{\text{SR}}(t)$ can be determined by the following equations, where $t_\phi = \frac{1}{2f_{\text{sw}}} - t_1$:

$$i_{\text{SR}}(t) = n\left[I_1 \cos\left(\frac{t}{\sqrt{L_r C_r}}\right) - \frac{nV_{\text{out}}t}{L_m} - I_{L_{m1}} - (V_1 - V_{\text{in}} + nV_{\text{out}})\sqrt{\frac{C_r}{L_r}}\sin\left(\frac{t}{\sqrt{L_r C_r}}\right)\right] \quad (1)$$

$$i_{\text{SR}}(t) = n\left[-I_0 \cos\left(\frac{t - t_\phi}{\sqrt{L_r C_r}}\right) - \frac{nV_{\text{out}}(t - t_\phi)}{L_m} + I_{L_{m0}} + (V_0 - V_{\text{in}} - nV_{\text{out}})\sqrt{\frac{C_r}{L_r}}\sin\left(\frac{t - t_\phi}{\sqrt{L_r C_r}}\right)\right]. \quad (2)$$

For the SR time-domain equations expressed in (1) and (2) to be solely a function of design parameters and known operating conditions, the unknown values $I_{L_{m1}}$, I_1, V_1, $I_{L_{m0}}$, I_0, V_0, and t_1 must be determined, as well as V_{in} or V_{out}, depending on which parameter is known. Based on circuit constraints, the unknown parameters can be calculated as follows:

$$I_{L_{m1}} = I_1 = -\frac{nV_{\text{out}}}{4L_m f_{\text{sw}}} \quad (3)$$

$$V_1 = V_{\text{in}} - nV_{\text{out}} - \frac{B}{m}nV_{\text{out}}\tan(A - B) - \frac{V_{\text{in}} - 2nV_{\text{out}}\cos(A)}{2\cos(B)\cos(A - B)} \quad (4)$$

$$I_{L_{m0}} = \frac{nV_{\text{out}}}{4L_m f_{\text{sw}}}\left(\frac{A}{B} - 1\right) \quad (5)$$

$$I_0 = -\sqrt{\frac{C_r}{L_r}}\left[\frac{2\frac{B}{m}nV_{\text{out}}\cos(B)}{2\cos(A - B)} + \frac{\sin(A)(2nV_{\text{out}}\cos(A - 2B) + V_{\text{in}})}{2\cos(B)\cos(A - B)}\right] \quad (6)$$

$$V_0 = V_{\text{in}} + nV_{\text{out}}(1 - 2\cos(A)) + \frac{\frac{B}{m}nV_{\text{out}}\sin(2B) + \cos(A)(2nV_{\text{out}}\cos(A) - V_{\text{in}})}{2\cos(B)\cos(A - B)} \quad (7)$$

$$\frac{V_{\text{out}}}{V_{\text{in}}} = -\frac{1}{2n}\frac{\sin(A - B)}{\frac{B}{m}\cos(B) + \sin(B)} \quad (8)$$

where $A = \frac{t_1}{\sqrt{L_r C_r}}$ and $B = \frac{1}{4f_{\text{sw}}\sqrt{L_r C_r}}$. For a given V_{in} and V_{out}, t_1 can be calculated from the equations presented. Otherwise, the loading condition needs to be provided so t_1 can be determined with

$$P_{\text{load}} = 4C_r f_{\text{sw}} V_{\text{in}}^2 \frac{\sin(A - B)\sin(\frac{A}{2} - B)\sin(\frac{A}{2})}{\frac{B}{m}(\cos(2B) + 1) + \sin(2B)}. \quad (9)$$

After the unknown parameters have been determined with (3)–(9), the expression for $i_{\text{SR}}(t)$ from (1) and (2) can be determined as a function of operating conditions and known design parameters.

B. Operation Below the Resonant Frequency

Waveforms for operation of the converter under this condition can be seen in Fig. 3. Once again, the average value of $v_C(t)$ is $\frac{V_{\text{in}}}{2}$ for $D = 0.5$, and the average value of both $i_{\text{tank}}(t)$ and $i_{L_m}(t)$ is zero. At $t = t_0 = 0$, $v_{\text{in}}(t)$ assumes the value V_{in}, which is maintained until $t = \frac{1}{2f_{\text{sw}}}$. The $v_{pr}(t)$ is maintained at nV_{out} from $t = t_0$ until $t = t_1$. At $t = t_1$, $v_{pr}(t)$ is no longer nV_{out}, but rather the voltage produced by i_{L_m}, since there is no current flowing through $i_{\text{TR}}(t)$ from $t = t_1$ to $t = \frac{1}{2f_{\text{sw}}}$. As a result, $i_{L_m}(t) = i_{\text{tank}}(t)$. As a result, the time-domain expression for the SR current for $0 < t < t_1$ can be determined with

$$i_{\text{SR}}(t) = n\left[I_0 \cos\left(\frac{t}{\sqrt{L_r C_r}}\right) - \frac{nV_{\text{out}}t}{L_m} - I_{L_{m0}} - (V_0 - V_{\text{in}} + nV_{\text{out}})\sqrt{\frac{C_r}{L_r}}\sin\left(\frac{t}{\sqrt{L_r C_r}}\right)\right]. \quad (10)$$

The unknown parameters $I_{L_{m0}}$, I_0, V_0, t_1, and V_{in} or V_{out} can be determined based on the established constraints as follows:

$$I_{L_{m0}} = I_0 \quad (11)$$

$$I_0 = \sqrt{\frac{C_r}{L_r}}\left[\frac{nV_{\text{out}}(1 + \cos(T)) - V_{\text{in}}}{\sqrt{m + 1}\sin(T) + \tan(\frac{A}{2})(\cos(T) - 1)} + \frac{\frac{A}{m}nV_{\text{out}}(\cos(T)\cot(A) - \sqrt{m + 1}\sin(T) + \csc(A))}{\sqrt{m + 1}\sin(T) + \tan(\frac{A}{2})(\cos(T) - 1)}\right] \quad (12)$$

$$V_0 = V_{\text{in}} - nV_{\text{out}} + \frac{\frac{A}{m}nV_{\text{out}}(\cos(T) + \sqrt{m + 1}\sin(T)\cot(A))}{\tan(\frac{A}{2})(1 - \cos(T)) - \sqrt{m + 1}\sin(T)} + \frac{(V_{\text{in}} - nV_{\text{out}}(\cos(T) + 1))}{(\cos(T) - 1) + \sqrt{m + 1}\cot(\frac{A}{2})\sin(T)} \quad (13)$$

$$\frac{V_{\text{out}}}{V_{\text{in}}} = \frac{\frac{m}{An}}{\frac{2m}{A} + \cot(\frac{A}{2}) - \sqrt{m + 1}\tan(\frac{T}{2})} \quad (14)$$

where $A = \frac{t_1}{\sqrt{L_r C_r}}$ and $T = \frac{1}{\sqrt{(L_r + L_m)C_r}}(\frac{1}{2f_{\text{sw}}} - t_1)$. For a given V_{in} and V_{out}, t_1 can be calculated numerically from (14).

Otherwise, it can be determined with

$$P_{\text{load}} = C_r f_{\text{sw}} V_{\text{in}}^2 \frac{K_1 K_2}{K_3 + K_4 + K_5 - \sqrt{m+1}\,(K_6 + K_7)} \tag{15}$$

where

$$\begin{cases} K_1 = \sqrt{1+m} - \tan\left(\frac{T}{2}\right)\tan\left(\frac{A}{2}\right) \\ K_2 = \frac{A}{2}\cot\left(\frac{A}{2}\right) - 1 \\ K_3 = \frac{A}{m}\left(\frac{\cos(A)+\cos(T)-2\cos(A)\cos(T)-2}{\sin(T)(\cos(A)-1)}\right) \\ K_4 = \frac{1+\frac{A}{2}\cot(\frac{A}{2})+m}{\tan(\frac{A}{2})\tan(\frac{A}{2\sqrt{1+m}})} \\ K_5 = \tan\left(\frac{T}{2}\right)\left(\tan\left(\frac{A}{2}\right) + A\right) \\ K_6 = \frac{A}{m}\left(\frac{\cos(A)+\cos(T)+2\cos(A)\cos(T)+2}{\sin(A)(\cos(T)+1)}\right) \\ K_7 = \frac{A}{2}\cot\left(\frac{A}{2}\right) + 2 \end{cases}. \tag{16}$$

After the unknown parameters have been determined with (11)–(16), the expression for $i_{\text{SR}}(t)$ from (10) can be determined as a function of design parameters and operating conditions.

C. Operation at the Resonant Frequency

Waveforms for operation of the converter at f_{res} are shown in Fig. 3. Under this special case, $v_{\text{in}}(t)$ and $v_{pr}(t)$ are aligned, so the circuit can be analyzed in its entirety during one time period, $t_0 = 0 < t < \frac{1}{2f_{\text{sw}}}$. The time-domain expression for the SR current is

$$i_{\text{SR}}(t) = n\left[I_0 \cos\left(\frac{t}{\sqrt{L_r C_r}}\right) - \frac{nV_{\text{out}}t}{L_m} - I_{L_{m\,0}} - (V_0 - V_{\text{in}} + nV_{\text{out}})\sqrt{\frac{C_r}{L_r}}\sin\left(\frac{t}{\sqrt{L_r C_r}}\right)\right]. \tag{17}$$

The unknown parameters $I_{L_{m\,0}}$, I_0, V_0, and V_{in} or V_{out} can be determined based on the established constraints as follows:

$$I_{L_{m\,0}} = I_0 = -\frac{nV_{\text{out}}\pi\sqrt{L_r C_r}}{2L_m} \tag{18}$$

$$V_0 = \frac{V_{\text{in}}}{2} - \pi\sqrt{\frac{L_r}{C_r}}\frac{P_{\text{load}}}{V_{\text{in}}} \tag{19}$$

$$\frac{V_{\text{out}}}{V_{\text{in}}} = \frac{1}{2n}. \tag{20}$$

After the unknown parameters have been determined with (18)–(20), the expression for $i_{\text{SR}}(t)$ from (17) can be determined as a function of known parameters and operating conditions.

D. Validation of the RCE Equations

In order to validate the developed RCE, a comparison between calculated, simulated, and measured waveforms can be performed. Because $i_{\text{SR}}(t)$ is directly related to P_{mos}, accurate tracing of this waveform is fundamental. To evaluate the performance of the model under different operating conditions, an experimental setup was implemented with the design parameters listed in Table I. Measurements of $i_{\text{SR}}(t)$ are shown for operation under different operating frequencies and loading conditions in Fig. 4, along with the waveforms calculated using the developed RCE and simulated results. Even though RCE considers an ideal transformer without leakage inductance L_r, simulation was performed considering $L_r = 2\%$. It is possible to observe a substantial similarity between the shape and magnitude of the simulated, calculated, and measured waveforms, with deviations of less than 5% between registered peak values of i_{SR}. In addition, different combinations of parameters were considered, including operating conditions with quality factor close to unity, and RCE was able to closely correlate to simulation waveforms in all considered scenarios.

TABLE I
LLC DESIGN PARAMETERS

Parameter	Value
Input Voltage (V_{in})	400 V
Nominal Power (P_{nom})	650 W
Nominal Load Voltage (V_{nom})	24 V
Switching Frequency (f_{sw})	150-250 kHz
Magnetizing Inductance (L_m)	103.4 μH
Resonant Inductance (L_r)	37.7 μH
Resonant Capacitance (C_r)	18.8 nF
Transformer Turns Ratio (n)	8.1

III. *LLC* SR TURN-ON AND TURN-OFF DELAYS: RCE VERSUS FHA

In *LLC* SR, the delay time (t_d) for turn-ON ($t_{d(\text{on})}$) or turn-OFF ($t_{d(\text{off})}$) is of paramount importance since power losses in SR MOSFETs (P_{mos}) increase during these periods, as Fig. 1 shows. These delays arise from measurement uncertainties and thresholds used in control algorithms, calculation and propagation delays, as well as safety margins to avoid shoot through. The calculation of P_{mos} using RCE allows for the incorporation of losses due to these delays, which increases the precision of loss calculation, facilitating the thermal management design of SR MOSFETs. During t_d, the body diode of the switches conducts, so its voltage drop (v_d) can be used as a function of parameters such as drain current (I_D) and junction temperature (T_j) for loss assessment. The P_{mos} for operation above and at f_{res} can be obtained as follows:

$$P_{\text{mos}} = f_{\text{sw}}\left[\int_0^{t_{d(\text{on})}} i_{\text{SR}} v_d dt + \int_{t_{d(\text{on})}}^{\frac{1}{2f_{\text{sw}}}-t_{d(\text{off})}} i_{\text{SR}}^2 R_{\text{DS(on)}} dt + \int_{\frac{1}{2f_{\text{sw}}}-t_{d(\text{off})}}^{\frac{1}{2f_{\text{sw}}}} i_{\text{SR}} v_d dt\right] \tag{21}$$

where $i_{\text{SR}}(t)$ is obtained from (1) and (2) for $f_{\text{sw}} > f_{\text{res}}$ and from (17) for $f_{\text{sw}} = f_{\text{res}}$. The expression for P_{mos} for the

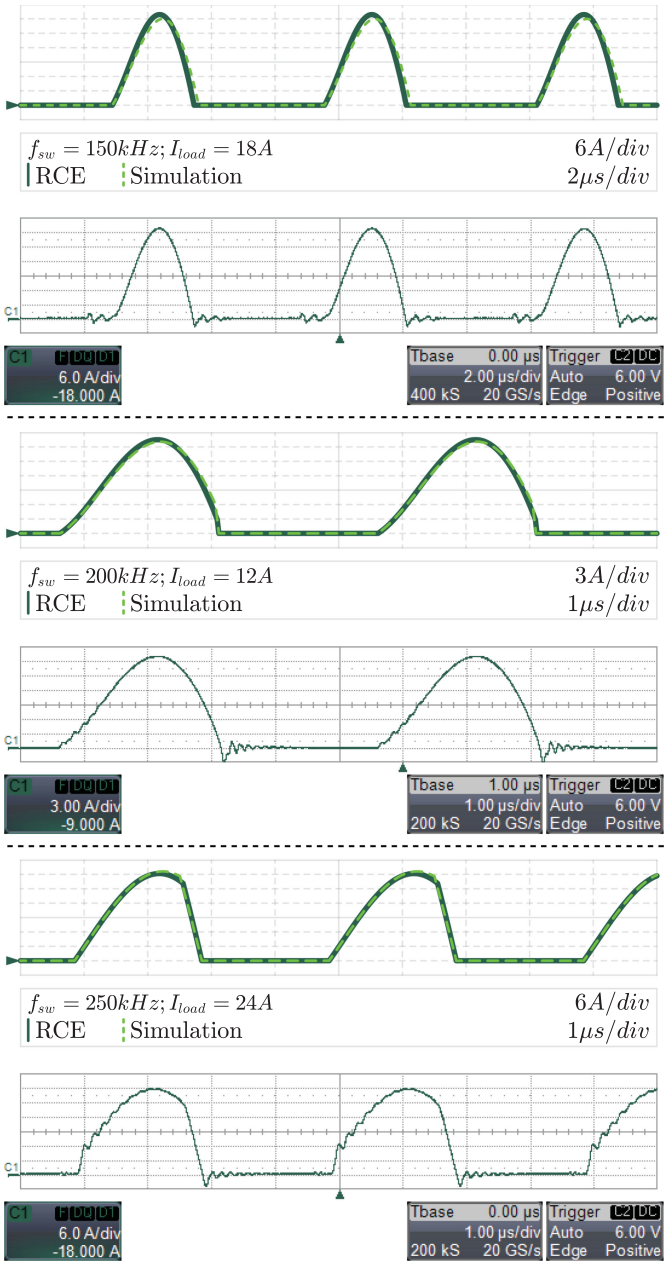

Fig. 4. Calculated and simulated $i_{\mathrm{SR}}(t)$ for given operating conditions closely correlate to waveforms obtained in experimental results.

converter operating below f_{res} can then be obtained as follows:

$$P_{\mathrm{mos}} = f_{\mathrm{sw}}\left[\int_{0}^{t_{d(\mathrm{on})}} i_{\mathrm{SR}} v_d dt + \int_{t_{d(\mathrm{on})}}^{t_1 - t_{d(\mathrm{off})}} i_{\mathrm{SR}}^2 R_{\mathrm{DS(on)}} dt + \int_{t_1 - t_{d(\mathrm{off})}}^{t_1} i_{\mathrm{SR}} v_d dt\right] \tag{22}$$

where the expression for $i_{\mathrm{SR}}(t)$ is determined by (10).

Due to the geometry of $i_{\mathrm{SR}}(t)$, the same variation in $t_{d(\mathrm{on})}$ is not as impactful in P_{mos} as it is for $t_{d(\mathrm{off})}$, independently of f_{sw}, as can be seen in Fig. 5(a). Since $i_{\mathrm{SR}}(t)$ presents a steeper

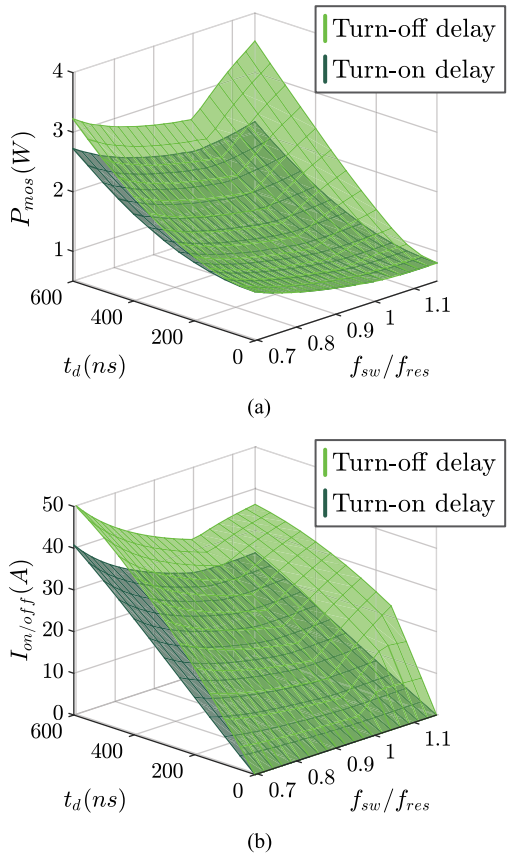

Fig. 5. (a) $t_{d(\mathrm{off})}$ is more critical for P_{mos} due to the geometry of $i_{\mathrm{SR}}(t)$, especially for $f_{\mathrm{sw}} > f_{\mathrm{res}}$. (b) I_{off} is higher than I_{on}, regardless of the f_{sw}.

slope during the second half of the waveform, the resulting current level at turn-ON (I_{on}) is lower than at turn-OFF (I_{off}) for the same t_d, as shown in Fig. 5(b). Thus, control strategies with higher $t_{d(\mathrm{off})}$ result in larger P_{mos}, especially for operation above f_{res}.

This behavior is not observed when FHA is employed to approximate $i_{\mathrm{SR}}(t)$, since FHA produces symmetric waveforms. In fact, a common practice is to assume that the ON-time (t_{on}) of the SR is fixed for operation below the resonant frequency at $t_{\mathrm{on}} = \pi\sqrt{L_r C_r}$. This produces a waveform that is closer in magnitude and shape to that observed in the real circuit, as shown in Fig. 6. Nevertheless, the waveform produced is symmetrical from $t = 0$ to $t_{\mathrm{on}} = \pi\sqrt{L_r C_r}$, and thus, cannot replicate the effect observed in Fig. 5. As a result, the prediction of P_{mos} using FHA is compromised.

IV. Design Considerations for P_{mos}

As observed previously, while FHA provides valuable insights regarding the operation of the *LLC* resonant converter, it lacks the level of detail required to accurately determine P_{mos} when compared with RCE. The incorporation of different t_d can further increase the difference observed using the two methods. In addition, different design considerations, such as choice of the inductance ratio m, may not be accounted for with FHA. It

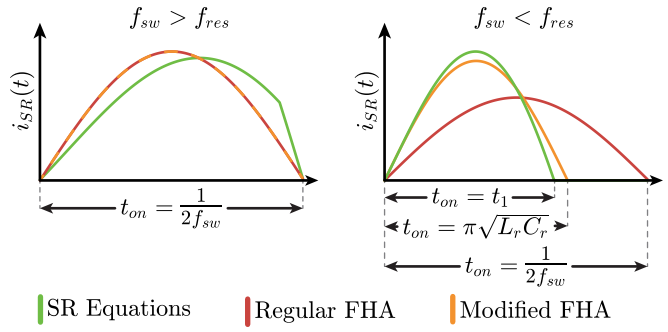

Fig. 6. While FHA generates perfectly sinusoidal waveforms (red), the $i_{\mathrm{SR}}(t)$ from RCE are not symmetrical (green). If t_{on} is fixed at $\pi\sqrt{L_r C_r}$ for $f_{\mathrm{sw}} < f_{\mathrm{res}}$ (orange), a better approximation of the waveform is obtained.

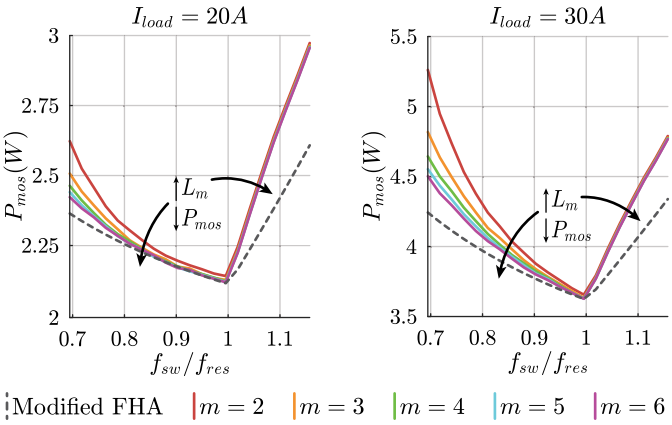

Fig. 7. RCE considers the impact of m for the determination of P_{mos}, which is not possible when employing FHA. Increased L_m results in smaller values of P_{mos}, which are underestimated using modified FHA.

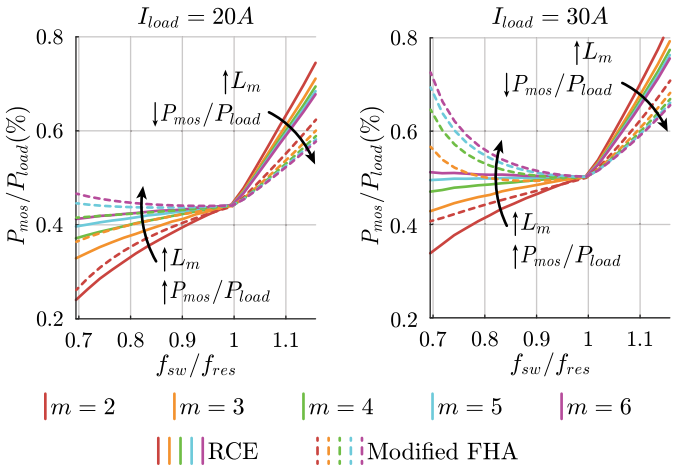

Fig. 8. Higher levels of $P_{\mathrm{mos}}/P_{\mathrm{load}}$ are observed at heavier loads. For $f_{\mathrm{sw}} < f_{\mathrm{res}}$, smaller values of L_m result in better efficiency, and for $f_{\mathrm{sw}} > f_{\mathrm{res}}$, higher values of L_m present a better performance.

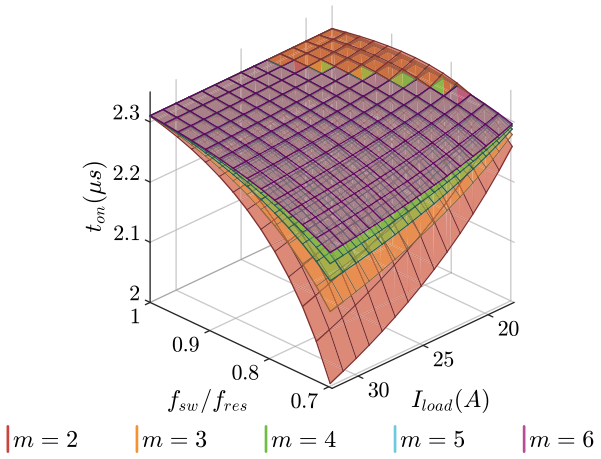

Fig. 9. t_{on} of SR MOSFETs depends on operating conditions, such as f_{sw} and I_{load}, and also on design considerations, such as inductance ratio m.

is known that this parameter in particular influences the electrical behavior of the converter, especially when it comes to the relationship between f_{sw} and V_{out}. While RCE is able to determine $i_{\mathrm{SR}}(t)$ with accuracy, considering the dependence of m for P_{mos} estimation, FHA only provides a single P_{mos} estimation for different m, as shown in Fig. 7.

When the converter operates below f_{res}, larger values of m, such as $m = 6$, will result in smaller P_{mos}, and the value obtained with the SR equations will approximate the value determined with FHA. Nevertheless, FHA provides a low prediction of P_{mos}, with increased discrepancy at heavier loading conditions. For operation above f_{res}, similar values are obtained with RCE for P_{mos} under different values of m, but larger values of m still result in slightly lower P_{mos}. FHA, on the other hand, underestimates P_{mos} under any operating condition, which can be detrimental to MOSFET selection.

Even though lower values of m result in larger P_{mos}, the power transferred to the load (P_{load}) differs from case to case, since the output voltage of the converter (V_{out}) depends on m. Therefore, it is important to analyze the ratio of power being dissipated in an SR MOSFET versus the total power being transferred to the load, namely $P_{\mathrm{mos}}/P_{\mathrm{load}}$. As seen before, the determination of P_{mos} using FHA does not depend on m, unlike what is seen in RCE. However, the calculation of P_{load} depends on this parameter using either FHA or RCE. As a result, different values of $P_{\mathrm{mos}}/P_{\mathrm{load}}$ can be obtained for various m using both methods: RCE and modified FHA.

Fig. 8 shows different levels of $P_{\mathrm{mos}}/P_{\mathrm{load}}$ for different loading conditions, estimation methods, and values of m, considering a 500 ns $t_{d(\mathrm{on})}$ and $t_{d(\mathrm{off})}$. Considering the results obtained with RCE, which are verified with simulation, it is possible to observe that the ratio $P_{\mathrm{mos}}/P_{\mathrm{load}}$ is higher at heavier loading conditions, which implies that the contribution of power losses from the SR of the *LLC* increases more significantly than the power transferred does. For operation below f_{res}, lower values of m yield better performance, while for operation above f_{res}, higher values of m are more efficient. This can be of interest when designing a converter that will more likely have a step-up or step-down operation, since it can assist in reducing losses in the SR stage independently of the control strategy employed.

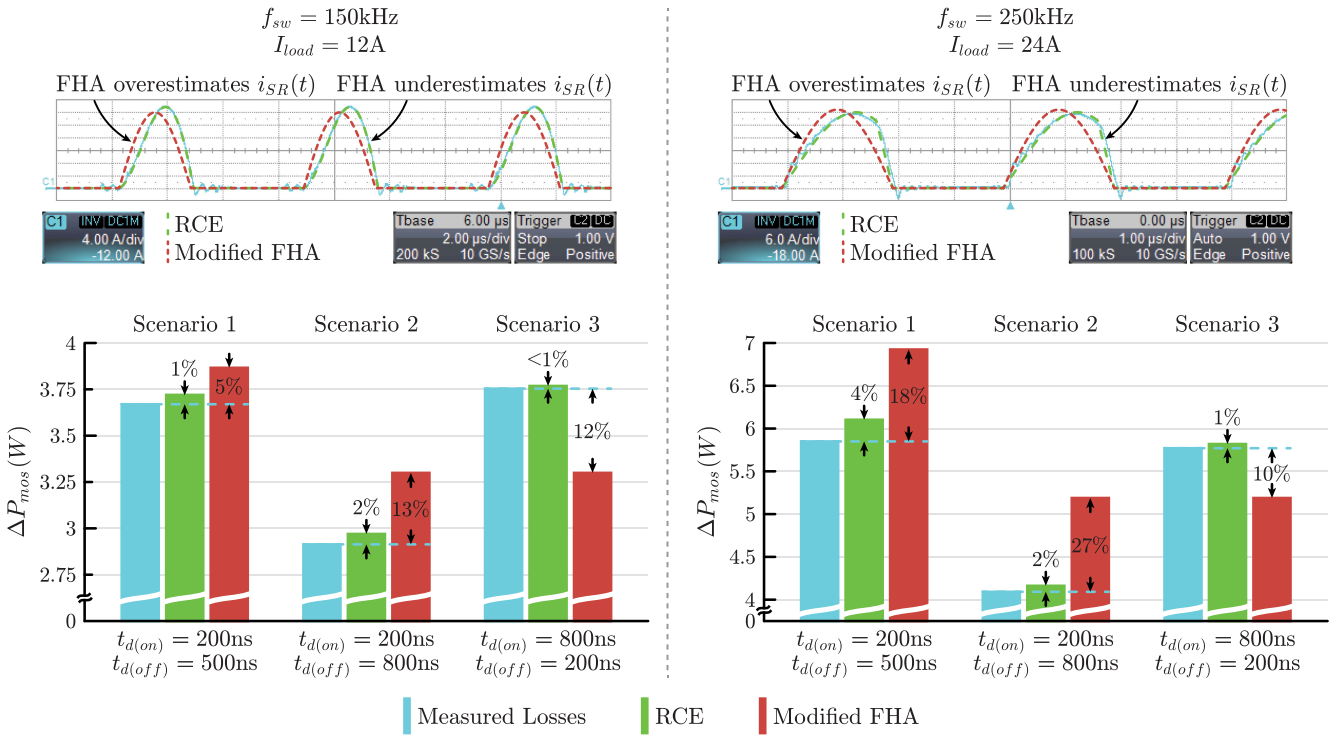

Fig. 10. Close correlation between experimental measurements and calculations using RCE is obtained for different values of $f_{\rm sw}$, $I_{\rm load}$, $t_{d(\rm on)}$, and $t_{d(\rm off)}$. The simplified FHA yields inaccurate results both in $\Delta P_{\rm mos}$ and in the obtained waveforms.

When considering the result obtained with FHA, it is possible to observe a similar trend. However, when comparing both results with RCE and FHA for the same value of m, it is possible to observe a considerable discrepancy, especially when the converter operates under a heavy loading condition and with high values of m. Therefore, FHA is not the best approach to determine $P_{\rm mos}$ accurately, especially for lower values of m, and it cannot determine $P_{\rm mos}/P_{\rm load}$ with precision for higher values of m. It is important to emphasize that the choice of m impacts not only the losses in the rectifying MOSFETs but also the general behavior of the topology, and a holistic approach must be considered in the selection of this parameter.

Another limitation of FHA is the determination of the $t_{\rm on}$ during which each MOSFET should conduct. The $t_{\rm on}$ can vary considerably for operation below $f_{\rm res}$, as shown in Fig. 9, and it depends on operating conditions, such as $I_{\rm load}$ and $f_{\rm sw}$, and on design parameters, such as m. Because FHA only considers a fixed $t_{\rm on} = \pi\sqrt{L_r C_r}$, it is not an adequate tool for predicting the actual conduction time of the SR MOSFETs, and thus, does not allow for a good estimation of $P_{\rm mos}$ when using different control techniques. As an alternative, RCE can be used to analyze the impact of different control techniques in $P_{\rm mos}$.

V. Experimental Power Loss Validation

In order to verify the effectiveness of the developed model in predicting $P_{\rm mos}$ under different operating conditions, the prototype with parameters listed in Table I was used. As observed in Section IV, smaller values of m result in $P_{\rm mos}$ estimations, which are substantially different from those predicted by FHA, as can be seen in Fig. 7. In this circuit $m = 2.74$, so it is expected that FHA will not be able to yield precise $P_{\rm mos}$ values, especially for operation above the resonant frequency.

In addition, as observed in Section III, $t_{d(\rm off)}$ is more critical than $t_{d(\rm on)}$. Moreover, different combinations of $t_{d(\rm on)}$ and $t_{d(\rm off)}$ result in different predictions of $P_{\rm mos}$, as can be observed in different SR control algorithms. In order to investigate these behaviors, the SR MOSFETs were controlled manually; so no specific control algorithm was employed.

Since the direct measurement of $P_{\rm mos}$ is not straightforward due to the high-frequency switching of the MOSFETs, instead the difference between $P_{\rm mos}$ when the SR is active or OFF was considered, which can be measured at ease using a high-precision power analyzer. This difference $\Delta P_{\rm mos}$ can be achieved by monitoring the $P_{\rm in}$ and $P_{\rm load}$ of the circuit when the SR is turned ON or OFF manually. Selected results are shown in Fig. 10, along with the comparison between measured losses and estimated values using RCE and modified FHA. In addition, a thermal camera was employed to monitor the operating temperature of the MOSFETs, as shown in Fig. 11, and different heat dissipation levels were observed as $P_{\rm mos}$ varied with the different operating conditions.

From Fig. 10, it is possible to conclude that the modified FHA produces current values that are greater in magnitude than those obtained using RCE or experimentally during the first half of the waveform. During the second half, RCE produces currents that are in accordance with experimental measurements, whereas FHA underestimates the current values. As a result,

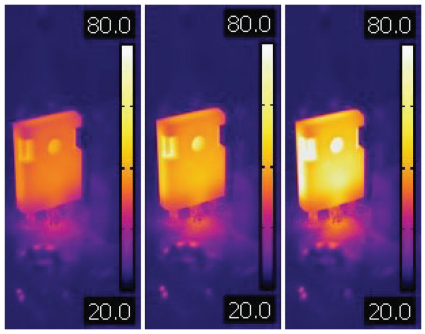

Fig. 11. Thermal camera images showing different heat dissipation levels for various P_{mos}.

ΔP_{mos} is overestimated by FHA when $t_{d(\mathrm{off})}$ is large, and underestimated with a smaller $t_{d(\mathrm{on})}$. This behavior is observed by comparing scenarios 2 and 3 provided in Fig. 10. It is also possible to observe that the measured ΔP_{mos} for $t_{d(\mathrm{on})} = 200$ ns and $t_{d(\mathrm{off})} = 500$ ns (see scenario 1) is comparable to that presented by $t_{d(\mathrm{on})} = 800$ ns and $t_{d(\mathrm{off})} = 200$ ns (see scenario 3). This reflects the fact that $t_{d(\mathrm{on})}$ is not as impactful in P_{mos} as $t_{d(\mathrm{off})}$ is. This becomes clear when $t_{d(\mathrm{on})}$ is maintained fixed at 200 ns and $t_{d(\mathrm{off})}$ is increased from 500 (see scenario 1) to 800 ns (see scenario 2). Such small change in $t_{d(\mathrm{off})}$ from 500 to 800 ns produces a significant drop in the efficiency of the converter, as shown by the bar graphs. This behavior also indicates the importance of a good control algorithm for the *LLC* SR, which may be necessary, especially for cases such as the one presented, where m is rather small.

Considering all the measurements performed, it was found that the maximum error presented between measured ΔP_{mos} and the calculation using RCE is 5%, while using modified FHA yielded in a maximum error of 37%. Considering the measured operating conditions, the average error presented was reduced from 12 to 2% by employing RCE instead of FHA. The inaccuracy of using FHA to determine P_{mos} becomes more critical for operation at $f_{\mathrm{sw}} = 250$ kHz, where the average error presented is of 18%, versus the 3%, obtained with RCE. This is in accordance with the findings from Section IV, and can also be observed in the waveforms provided in Fig. 10. Simulation results employing $L_r = 2\%$ also indicate a close correlation with the obtained results using RCE, for an error of no more than 3% for the considered scenarios.

VI. Conclusion

This paper presented a method for estimating power losses in *LLC* SR MOSFETs (P_{mos}) based on the RCE of the topology. Unlike most of the literature in this field, the method presented is not a control algorithm but a tool that can assist in determining P_{mos} before the converter is built, and with improved accuracy when compared with the established yet oversimplified FHA. The developed RCE method allows for the study of the performance of the SR considering different operating conditions and design parameters.

Aspects such as the impact of inductance ratio (m) and different turn-ON and turn-OFF delays (t_d) were studied. It was noted that small values of m require a more elaborate SR control algorithm, and that the impact of $t_{d(\mathrm{off})}$ in P_{mos} was more pronounced when compared with $t_{d(\mathrm{on})}$. These phenomena cannot be observed when employing FHA due to the oversimplification of this method.

Improved correlation with experimental measurements and simulation results was obtained using RCE when compared with FHA. A reduction from 12% to 2% in average power loss estimation error was obtained, which is fundamental in applications such as component selection and thermal management design. RCE was implemented in MS Excel and based on over 400 operating conditions, the average P_{mos} calculation time was of only 2.2 s per operating condition, versus an average of 110 s when using simulation software. This considerable reduction in calculation time allows for the determination of P_{mos} and operating temperatures under various conditions, which is fundamental for applications such as battery charging, where operating conditions vary considerably over time.

References

[1] K. W. E. Cheng and P. D. Evans, "Parallel-mode extended-period quasiresonant convertor," *IEE Proc. B—Elect. Power Appl.*, vol. 138, no. 5, pp. 243–251, Sep. 1991.

[2] R. C. N. Pilawa-Podgurski, A. D. Sagneri, J. M. Rivas, D. I. Anderson, and D. J. Perreault, "Very-high-frequency resonant boost converters," *IEEE Trans. Power Electron.*, vol. 24, no. 6, pp. 1654–1665, Jun. 2009.

[3] G. Yang, P. Dubus, and D. Sadarnac, "Double-phase high-efficiency, wide load range high-voltage/low-voltage LLC dc/dc converter for electric/hybrid vehicles," *IEEE Trans. Power Electron.*, vol. 30, no. 4, pp. 1876–1886, Apr. 2015.

[4] F. Musavi, M. Craciun, D. S. Gautam, W. Eberle, and W. G. Dunford, "An LLC resonant dc-dc converter for wide output voltage range battery charging applications," *IEEE Trans. Power Electron.*, vol. 28, no. 12, pp. 5437–5445, Dec. 2013.

[5] C. Duan, H. Bai, W. Guo, and Z. Nie, "Design of a 2.5-kW 400/12-V high-efficiency dc/dc converter using a novel synchronous rectification control for electric vehicles," *IEEE Trans. Transport. Electrific.*, vol. 1, no. 1, pp. 106–114, Jun. 2015.

[6] X. Sun, Y. Shen, Y. Zhu, and X. Guo, "Interleaved boost-integrated LLC resonant converter with fixed-frequency PWM control for renewable energy generation applications," *IEEE Trans. Power Electron.*, vol. 30, no. 8, pp. 4312–4326, Aug. 2015.

[7] S. D. Mauro, S. Musumeci, A. Raciti, F. Fusillo, F. Scrimizzi, and R. Scollo, "Synchronous rectification with low voltage MOSFETS in LLC converters," in *Proc. AEIT Int. Annu. Conf.*, Sep. 2017, pp. 1–6.

[8] C. Zheng, B. Chen, L. Zhang, R. Chen, and J. S. Lai, "Design considerations of LLC resonant converter for contactless laptop charger," in *Proc. IEEE Appl. Power Electron. Conf. Expo.*, Mar. 2015, pp. 3341–3347.

[9] S. Abe *et al.*, "Sensing-less drive of synchronous rectifier for LLC resonant converter," in *Proc. Intelec*, Sep. 2012, pp. 1–6.

[10] S. Abe *et al.*, "Adaptive driving of synchronous rectifier for LLC converter without signal sensing," in *Proc. 28th Annu. IEEE Appl. Power Electron. Conf. Expo.*, Mar. 2013, pp. 1370–1375.

[11] J. Wang and B. Lu, "Open loop synchronous rectifier driver for LLC resonant converter," in *Proc. 28th Annu. IEEE Appl. Power Electron. Conf. Expo.*, Mar. 2013, pp. 2048–2051.

[12] L. Hong, H. Ma, J. Wang, J. Du, and B. Wang, "An efficient algorithm strategy for synchronous rectification used in LLC resonant converters," in *Proc. 42nd Annu. Conf. IEEE Ind. Electron. Soc.*, Oct. 2016, pp. 2452–2456.

[13] M. Mohammadi, N. Shafiei, and M. Ordonez, "LLC synchronous rectification using coordinate modulation," in *Proc. IEEE Appl. Power Electron. Conf. Expo.*, Mar. 2016, pp. 848–853.

[14] C. Zhao, B. H. Li, J. Cao, Y. Chen, X. Wu, and Z. Qian, "A novel primary current detecting concept for synchronous rectified LLC resonant converter," in *Proc. IEEE Energy Convers. Congr. Expo.*, Sep. 2009, pp. 766–770.

[15] X. Xie, J. C. P. Liu, F. N. K. Poon, and M. H. Pong, "A novel high frequency current-driven synchronous rectifier applicable to most switching topologies," *IEEE Trans. Power Electron.*, vol. 16, no. 5, pp. 635–648, Sep. 2001.
[16] J. Liao, J. Wang, J. Zhang, and Z. Qian, "A novel current driving scheme for LLC resonant converter with synchronized voltage-doubler rectifier," in *Proc. 26th Annu. IEEE Appl. Power Electron. Conf. Expo.*, Mar. 2011, pp. 566–570.
[17] X. Wu, B. Li, Z. Qian, and R. Zhao, "Current driven synchronous rectifier with primary current sensing for LLC converter," in *Proc. IEEE Energy Convers. Congr. Expo.*, Sep. 2009, pp. 738–743.
[18] B.-C. Kim, H.-S. Park, S. C. Moon, Y.-D. Kim, D.-Y. Kim, and G. W. Moon, "The novel synchronous rectifier driving method for LLC series resonant converter," in *Proc. 38th Annu. Conf. IEEE Ind. Electron. Soc.*, Oct. 2012, pp. 810–813.
[19] X. Huang, J. Wang, J. Zhang, and Z. Qian, "A hybrid driving scheme for full-bridge synchronous rectified LLC resonant dc/dc converter," in *Proc. 26th Annu. IEEE Appl. Power Electron. Conf. Expo.*, Mar. 2011, pp. 579–584.
[20] A. Lokhandwala, M. Salato, and M. Soldano, "Dual smartrectifier and directfet chipset overcomes package source inductance effects and provides accurate sensing for synchronous rectification in dc-dc resonant converters," in *Proc. 22nd Annu. IEEE Appl. Power Electron. Conf. Expo.*, Feb. 2007, pp. 1559–1562.
[21] B. Agrawal, M. Preindl, B. Bilgin, and A. Emadi, "Estimating switching losses for SiC MOSFETS with non-flat miller plateau region," in *Proc. IEEE Appl. Power Electron. Conf. Expo.*, Mar. 2017, pp. 2664–2670.
[22] P. G. Neudeck, R. S. Okojie, and L.-Y. Chen, "High-temperature electronics—A role for wide bandgap semiconductors?" *Proc. IEEE*, vol. 90, no. 6, pp. 1065–1076, Jun. 2002.
[23] E. S. Glitz, M. Amyotte, M. C. G. Perez, and M. Ordonez, "LLC converters: Beyond datasheets for MOSFETS power loss estimation," in *Proc. IEEE Appl. Power Electron. Conf. Expo.*, Mar. 2018, pp. 464–468.
[24] H.-J. Jiang, G. Maggetto, and P. Lataire, "Steady-state analysis of the series resonant dc-dc converter in conjunction with loosely coupled transformer-above resonance operation," *IEEE Trans. Power Electron.*, vol. 14, no. 3, pp. 469–480, May 1999.
[25] J. F. Lazar and R. Martinelli, "Steady-state analysis of the LLC series resonant converter," in *Proc. 16th Annu. IEEE Appl. Power Electron. Conf. Expo.*, 2001, vol. 2, pp. 728–735.
[26] X. Li and A. K. Rathore, "Steady-state analysis of a dual-bridge LLC inverter," in *Proc. 7th IEEE Conf. Ind. Electron. Appl.*, Jul. 2012, pp. 769–774.
[27] Z. Fang, S. Duan, C. Chen, X. Chen, and J. Zhang, "Optimal design method for LLC resonant converter with wide range output voltage," in *Proc. 28th Annu. IEEE Appl. Power Electron. Conf. Expo.*, Mar. 2013, pp. 2106–2111.
[28] W. Liu, B. Wang, W. Yao, Z. Lu, and X. Xu, "Steady-state analysis of the phase shift modulated LLC resonant converter," in *Proc. IEEE Energy Convers. Congr. Expo.*, Sep. 2016, pp. 1–5.
[29] Y. Shen, H. Wang, F. Blaabjerg, X. Sun, and X. Li, "Analytical model for LLC resonant converter with variable duty-cycle control," in *Proc. IEEE Energy Convers. Congr. Expo.*, Sep. 2016, pp. 1–7.
[30] M. Mohammadi and M. Ordonez, "Synchronous rectification of LLC resonant converters using homopolarity cycle modulation," *IEEE Trans. Ind. Electron.*, vol. 66, no. 3, pp. 1781–1790, Mar. 2019.

Ettore Scabeni Glitz (S'17) was born in Curitiba, Brazil. He received the B.Eng. degree in electrical engineering from the Federal University of Technology—Parana, Curitiba, Brazil, in 2016, and the M.A.Sc. degree in electrical and computer engineering from The University of British Columbia, Vancouver, BC, Canada, in 2019.

He is currently an Electrical Designer with AES Engineering, Vancouver, BC, Canada.

Jhih-Da Hsu (S'18) was born in Taichung City, Taiwan. He received the B.Sc. and the M.Sc. degree in electrical and control engineering from National Chiao Tung University, Hsinchu City, Taiwan, in 2005 and 2007, respectively. He is currently working toward the Ph.D. degree in electrical and computer engineering with the University of British Columbia (UBC), Vancouver, BC, Canada.

From 2008 to 2016, he was a System Engineer with Fairchild Semiconductor, Taipei, Taiwan, where he was responsible for the research and development of control ICs for laptop and smartphone chargers. Meanwhile, he is also a Research Scholar with Delta-Q Technologies, Burnaby, BC. His current research interests include medium- and high-power dc–dc resonant converters for electric vehicle battery chargers and renewable energy applications.

Martin Ordonez (S'02–M'09) was born in Neuquen, Argentina. He received the Ing. degree in electronics engineering from National Technological University, Cordoba, Argentina, in 2003, and the M.Eng. and Ph.D. degrees in electrical engineering from the Memorial University of Newfoundland (MUN), St. John's, NF, Canada, in 2006 and 2009, respectively.

He is currently a Professor and Canada Research Chair in Power Converters for Renewable Energy Systems with the Department of Electrical and Computer Engineering, University of British Columbia (UBC), Vancouver, BC. He is the Fred Kaiser Professor on Power Conversion and Sustainability with UBC. He was an Adjunct Professor with Simon Fraser University, Burnaby, BC and MUN. His industrial experience in power conversion includes research and development with Xantrex Technology Inc./Elgar Electronics Corp. (now AMETEK Programmable Power in San Diego, CA, USA). With the support of industrial funds and the Natural Sciences and Engineering Research Council, he has contributed to more than 150 publications and R&D reports.

Dr. Ordonez is a Guest Editor for the IEEE JOURNAL OF EMERGING AND SELECTED TOPICS IN POWER ELECTRONICS, an Associate Editor of the IEEE TRANSACTIONS ON POWER ELECTRONICS, and an Editor for the IEEE TRANSACTIONS ON SUSTAINABLE ENERGY. He serves on several IEEE committees, and reviews widely for IEEE/IET journals and international conferences. He was the recipient of the David Dunsiger Award for Excellence in the Faculty of Engineering and Applied Science (2009) and the Chancellors Graduate Award/Birks Graduate Medal (2006), and became a Fellow of the School of Graduate Studies, MUN.